SCIENCE AND TECHNOLOGY OF ADVANCED MATERIALS, 2018
VOL. 19, NO. 1, 44–52
https://doi.org/10.1080/14686996.2017.1410055

Taylor & Francis
Taylor & Francis Group

FOCUS ISSUE ARTICLE

OPEN ACCESS Check for updates

Mechanistic insights into water adsorption and dissociation on amorphous TiO_2-based catalysts

Kulbir Kaur Ghuman

International Institute for Carbon Neutral Energy Research, Kyushu University, Fukuoka, Japan

ABSTRACT

Despite having defects, amorphous titanium dioxide ($aTiO_2$) have attracted significant scientific attention recently. Pristine, as well as various doped $aTiO_2$ catalysts, have been proposed as the potential photocatalysts for hydrogen production. Taking one step further, in this work, the author investigated the molecular and dissociative adsorption of water on the surfaces of pristine and Fe^{2+} doped $aTiO_2$ catalysts by using density functional theory with Hubbard energy correction (DFT+U). The adsorption energy calculations indicate that even though there is a relatively higher spatial distance between the adsorbed water molecule and the $aTiO_2$ surface, pristine $aTiO_2$ surface is capable of anchoring H_2O molecule more strongly than the doped $aTiO_2$ as well as the rutile (1 1 0) surface. Further, it was found that unlike water dissociation on crystalline TiO_2 surfaces, water on pristine $aTiO_2$ catalyst experience the dissociation barrier. However, this barrier reduces significantly when $aTiO_2$ is doped with Fe^{2+}, providing an alternative route for the development of an inexpensive and more abundant catalyst for water splitting.

ARTICLE HISTORY
Received 27 June 2017
Revised 17 November 2017
Accepted 23 November 2017

KEYWORDS
Amorphous titanium dioxide; doping; catalyst; hydrogen; surface reaction

CLASSIFICATION
50 Energy Materials; 205 Catalyst / Photocatalyst / Photosynthesis

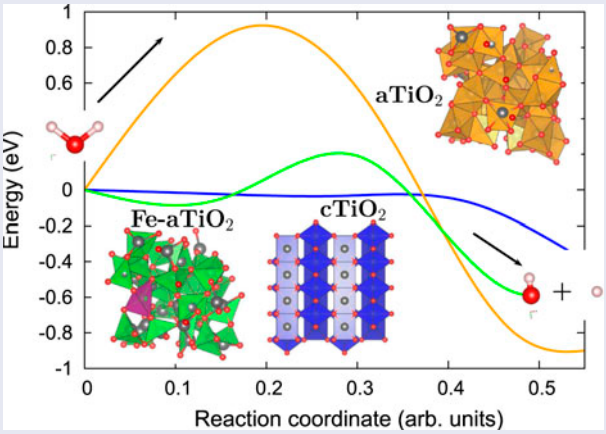

Graphical abstract showing the reduction in water splitting barrier due to doping in amorphous TiO_2, bringing the catalytic acivity of amorphous TiO_2 close to crystalline TiO_2.

1. Introduction

Among various oxide semiconductor photocatalysts, crystalline forms of titanium dioxide ($cTiO_2$) have attracted significant attention in last decades as promising photocatalysts due to its biological and chemical inertness, strong oxidizing power and long-term stability against photocorrosion and chemical corrosion [1,2]. Where many crystalline oxide surfaces [3] including $cTiO_2$ surfaces [4–6] are extensively studied for their electronic structures, defect levels and polaron formation, amorphous TiO_2 ($aTiO_2$) despite having actual technical applications such as use as an active photocatalyst, a substrate, or a protection layer [7–9] was lacking many such investigations until recently. It is now well known that there is a possibility of using $aTiO_2$ as an inexpensive and more abundant alternative to $cTiO_2$ [10,11] which may lead to relatively simple and inexpensive technology in future.

Despite having qualitatively similar electronic structure as of $cTiO_2$ [10,11], $aTiO_2$ forms large localized bound state on several O and Ti atoms due to the strong electron interaction with the lattice distortion [10,12,13]. These localized states in $aTiO_2$ leads to self-trapping of holes, excess electrons and excitons which play important roles in the radiation-induced processes [14–16] such as water splitting. Moreover, very recently

CONTACT Kulbir Kaur Ghuman kulbirghuman@i2cner.kyushu-u.ac.jp

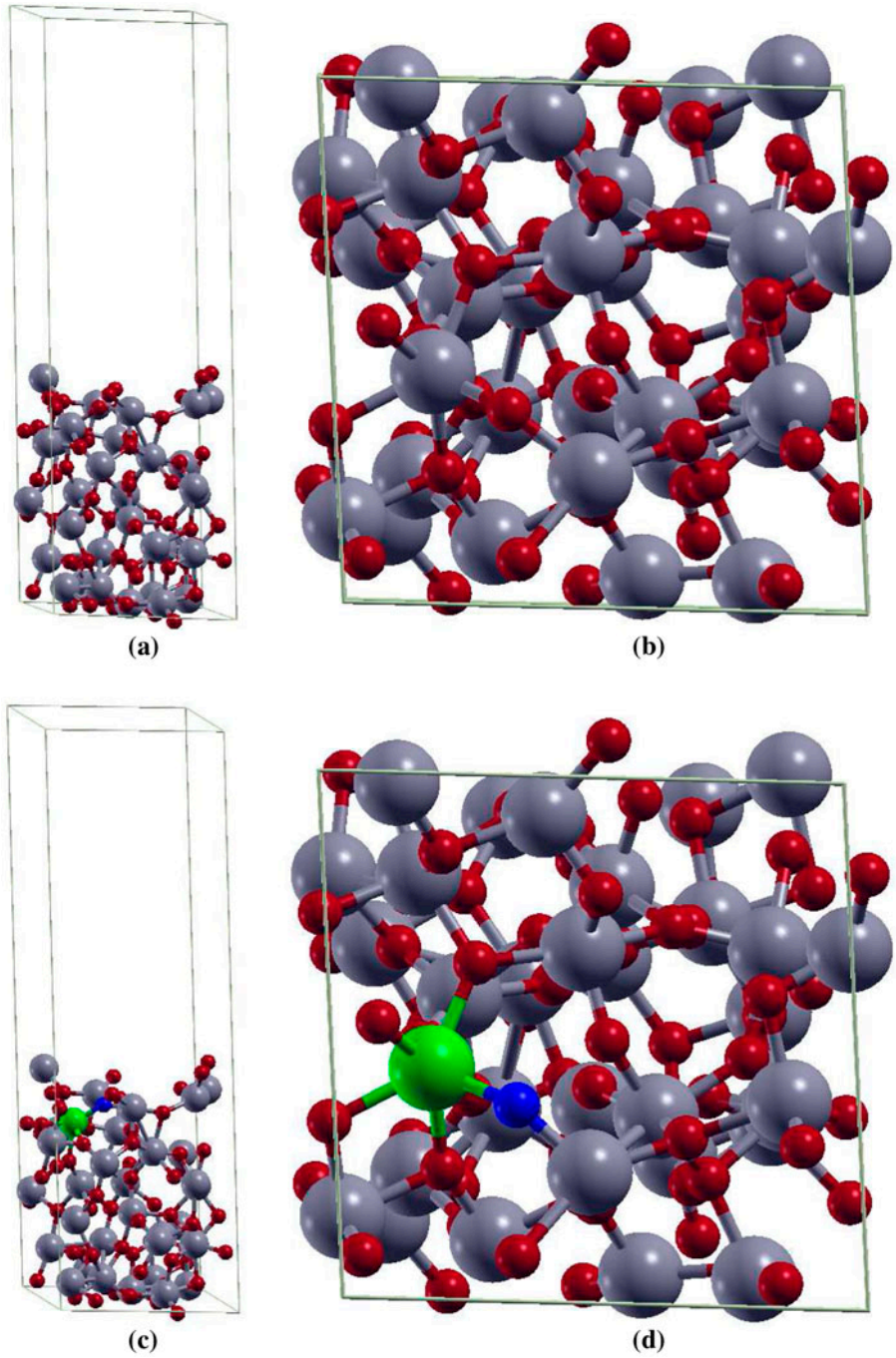

Figure 1. The (a) side and the (b) top view of 2 × 2 × 4 supercell of $aTiO_2$. The (c) side and the (d) top view of 2 × 2 × 4 supercell of Fe(II)-$aTiO_2$. Ti, O, Fe and O vacancy atoms are highlighted in grey, red, green, and blue, respectively.

many studies showed that the photoactivity of $aTiO_2$ can further be enhanced by doping it with suitable dopants [17–23]. The synergetic role that the amorphousness and dopants play in the photoactivity of $aTiO_2$ was attributed to the unique position of the midgap states, high self-trap energy, low mobility and weak chemical bonds of doped $aTiO_2$ [24].

Inspite of these numerous studies proposing $aTiO_2$-based catalysts for water splitting, the fundamental insights into the reaction pathway for water dissociation on $aTiO_2$-based catalysts are still lacking. This motivated the author to analyse the associative and dissociative water adsorption on pristine and doped $aTiO_2$ surfaces using first-principles based theoretical investigations. Since our recent study [24] clearly indicated that the visible light absorption of $aTiO_2$ can be improved by doping it with Fe^{2+} due to its unique properties, the author have considered Fe^{2+} doped $aTiO_2$ (Fe(II)-$aTiO_2$) as a model for doped $aTiO_2$ catalyst. Further in this work, the performance of $aTiO_2$-based catalysts is also compared with $cTiO_2$, by analysing water splitting on rutile (1 1 0) surface with the same level of theory.

2. Computational models and methods

The melt-quenching method was used to prepare $aTiO_2$ models [12]. The properties of the prepared $aTiO_2$

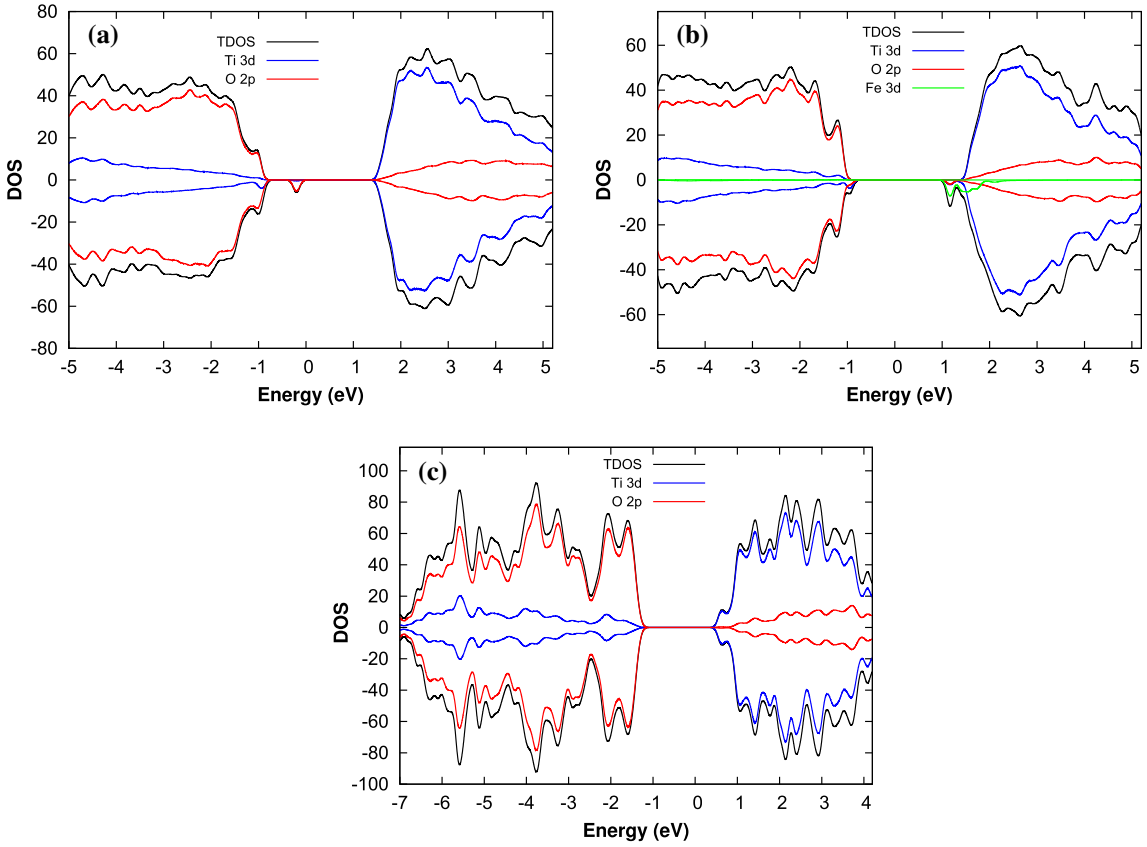

Figure 2. Total density of states and the projected density of states on the p and d orbitals of (a) $aTiO_2$, (b) Fe(II)-$aTiO_2$, and (c) rutile (1 1 0) surface models.

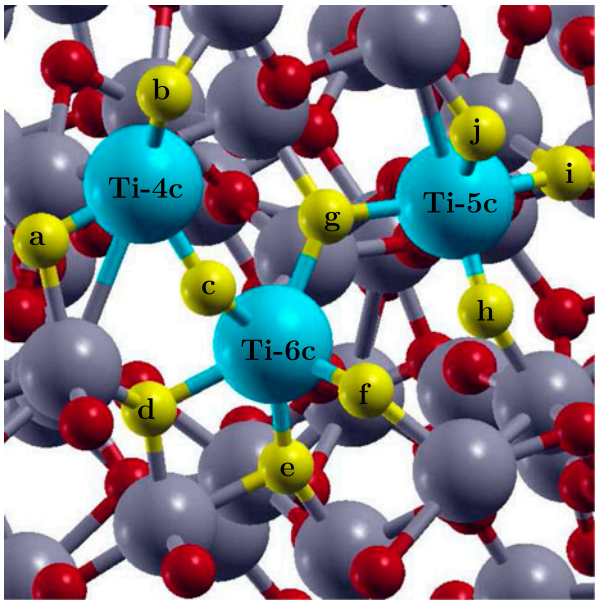

Figure 3. The $aTiO_2$ surface indicating the absorption sites for H_2O, OH and H species. Adsorption of H_2O and OH was investigated by placing them on the top of the Ti atoms indicated in blue and adsorption of H was investigated by placing it on the top of oxygen atoms indicated in yellow. Rest of the Ti and O atoms are highlighted in grey and red, respectively.

models are in agreement with experimental and theoretical data available. The structural analysis of these models suggests that local structural features of bulk $cTiO_2$ are retained in $aTiO_2$. In order to obtain the amorphous TiO_2 surface in the present study, a vacuum of about 20 Å is added in the z direction of $2 \times 2 \times 4$ bulk supercell (96-atom model) [25]. For doped $aTiO_2$ model, the author considered substitutional doping of a single Ti atom by one Fe atom and one O vacancy resulting into Fe(II) oxidation state with 3.125 at.% dopant concentration. The pristine $aTiO_2$ model and the doped $aTiO_2$ model indicating the positions of Fe atoms and O vacancy are shown in Figure 1. This doping level can be readily achieved for 3d transition metals in rutile TiO_2 [26,27].

The electronic characteristics of $aTiO_2$ sample has been investigated using *ab initio* method. The plane wave pseudopotential approach, together with the Perdew–Burke–Ernzerhof [28] exchange–correlation functional, and Vanderbilt ultrasoft pseudopotentials [29] was utilized throughout. The kinetic energy cutoffs of 544 and 5440 eV were used for the smooth part of the electronic wavefunctions and augmented electron density, respectively. The Quantum-ESPRESSO code, PWSCF package [30], was used to perform the calculations. All calculations are spin polarized. The structures were relaxed by using a conjugate gradient minimization algorithm until the magnitude of residual Hellman–Feynman force on each atom was less

than 10^{-2} Ry/Bohr. In all electronic density of states (DOS) and projected density of states (PDOS) plots a conventional Gaussian smearing of 0.007 Ry was utilized.

Appreciable underestimation of band gap and delocalization of d and f electrons are well-known limitations of DFT. Therefore, density functional theory with Hubbard energy correction (DFT+U) formalism was used in this study with $U = 4.2$ eV applied to Ti 3d electrons and $U = 6.00$ eV applied to Fe 3d electrons for analysing electronic properties of pristine and doped aTiO_2. The value of U for Ti has been chosen not solely on the basis of band gap but also depending on the property of interest [31], which in the current study, is the photocatalytic behaviour of TiO_2 that in-turn depends upon the position of band gap states and their effect on the electronic structure [32]. This value of U for Ti is consistent with theoretical investigations by Morgan et al. [33], who calculated it by fitting the peak positions for surface oxygen vacancies to experimental X-ray photoelectron spectroscopy data. Further the value of U for Fe is taken from Ref. [34] which showed that the DOS of FeO show characteristics similar to experiments [35] with $U = 6.0$ eV. Lastly, in order to evaluate the minimum energy pathways (MEPs) and transition states (TSs) for the water splitting reaction and estimate the relative activation energy barriers faced during dissociation of H_2O molecule, non-spin-polorized climbing image nudged elastic-band (CI-NEB) DFT calculations with 7 images [36–38] were performed.

3. Results and discussion

First, the electronic properties of pristine aTiO_2 and Fe(II)-aTiO_2 surfaces were analysed and compared with the electronic properties of rutile (1 1 0) surface. Then the active sites for the adsorption of H_2O, OH, and H species on pristine aTiO_2 and Fe(II)-aTiO_2 surfaces were investigated followed by the study of reaction mechanism for water splitting on them. Water splitting on rutile (1 1 0) surface was also analysed for comparison. One water molecule per unit cell was used for all the calculations.

3.1. Electronic properties of aTiO_2, Fe(II)-aTiO_2, rutile (1 1 0) surfaces

To understand the catalytic properties of amorphous and crystalline surfaces, the author first studied the electronic DOS and PDOS for the d electrons of Fe and Ti atoms and p electrons of O atoms for pristine aTiO_2, Fe(II)-aTiO_2, and rutile (1 1 0) surfaces. The DOS and PDOS are represented in Figure 2 for all the surfaces. It can be seen from Figure 2 that the magnitude of the Γ point electronic gap, defined as the difference between the highest occupied molecular orbital (HOMO) and the lowest unoccupied molecular orbital (LUMO), is about 2.2, 1.8, and 1.6 eV for pristine aTiO_2, Fe(II)-aTiO_2 and rutile (1 1 0) surfaces, respectively. Further, for all the surfaces the valence band mainly consists of the O 2p states and that the conduction band is dominated by Ti 3d states. In addition, the DOS analyses also reveals that there exist a midgap state for aTiO_2 surface due to O 2p orbitals (Figure 2(a)). However, it disappears when aTiO_2 is doped with Fe(II) (Figure 2 (b)). The midgap states can act as a recombination or a trapping center [24] and hence can decrease or increase the catalytic activity of aTiO_2 surface accordingly. The band tail states for Fe(II)-aTiO_2 surface however act as a trapping center and improve the photoactivity of Fe-aTiO_2 by absorbing light in visible region as reported in our previous study [24].

3.2. Adsorption energy calculation for H_2O, OH and H species

The adsorption energies of H_2O, OH and H species on the amorphous surfaces were calculated as

$$\delta H_{\text{ads}} = E_{\text{tot}} - E_{\text{bare}} - E_{ad} \quad (1)$$

where E_{tot} (E_{bare}) is the energy of the surface with (without) adsorbate and E_{ad} is the energy of the isolated adsorbate species calculated in the same supercell. Hence, a negative δH_{ads} indicates stable adsorption whereas a positive value indicates unstable adsorption. The author also calculated the adsorption of H_2O molecule and dissociated H_2O on rutile (1 1 0) surface for comparison. Adsorption energies for the most stable site for all the surfaces are represented in Table 1.

As a first step, author has investigated the possibility of H_2O, H and OH adsorption on the pristine aTiO_2 surface. For H_2O and OH adsorption a total of three surface Ti atom sites based on their different coordination number were identified: fourfold coordinated Ti (Ti-4c), fivefold coordinated Ti (Ti-5c) and sixfold coordinated Ti (Ti-6c). For H adsorption, all the O atom sites neighbouring to these three surface Ti atoms were investigated. The three sites for H_2O and OH adsorption and the ten sites for H adsorption are highlighted in Figure 3 in blue and yellow, respectively. While it is possible that the other adsorption sites exist on the aTiO_2 surface, the sites that author identified are enough to provide an understanding of the relative strength of binding and the spread of adsorption energies.

By analysing the interaction of H_2O molecule on the three adsorption sites, surprisingly, it was found that binding of H_2O with Ti-6c ($\delta H_{\text{ads}} = -1.07$ eV) is energetically preferred over under-coordinated Ti-5c ($\delta H_{\text{ads}} = -0.24$ eV) and Ti-4c sites ($\delta H_{\text{ads}} = -0.30$ eV). This result is contrary to the H_2O adsorption on cTiO_2 surfaces [39]. On crystalline surfaces water prefers to

Table 1. Calculated structural parameters and adsorption energies of H_2O, OH, and H for the most stable site on pristine $aTiO_2$, Fe(II)-$aTiO_2$ and rutile (1 1 0) surfaces. δH_{ads} (eV) represents the adsorption energy, h(Å) represents the vertical height of the H_2O, OH and H species from the nearest surface atom, d_{O-H} represents the OH bond lengths for OH and H_2O molecules and α_{HOH} represents the H–O–H angle for H_2O molecule.

Most stable species	H_{ads} (eV)	h(Å)	d_{O-H}	α_{HOH}
Pristine $aTiO_2$ surface				
H_2O (on site Ti-6c)	−1.072	3.519	1.055, 1.002	107.285
OH (on site Ti-4c)	−4.199	1.838	0.976	–
H (on site a)	−5.541	0.976	–	–
Fe(II)-$aTiO_2$ surface				
H_2O (on site Fe-6c)	−0.793	2.263	0.9978, 0.9878	104.716
OH (on site Fe-6c)	−1.288	2.069	0.994	–
H (on site c)	−4.807	0.977	–	–
Rutile (1 1 0) surface				
H_2O (on site Ti-5c)	−0.9378	2.212	0.979, 0.979	109.775
OH(on site Ti5c)-H (on bidentate O)	−8.503	1.822 (OH-surface), 0.973 (H-surface)	0.980 (O–H)	–

adsorb on under-coordinated site. To explain this, $aTiO_2$ surfaces before and after water adsorption on all the sites were analysed. It was found that the atoms neighbouring to Ti-6c rearrange themselves after water adsorbs on this site (Figure 4). For instance, the O atom (circled) neighbouring to Ti-6c site and showing charge accumulation (represented by spin density diagram, Figure 5(a)) gets rearranged after water adsorption on Ti-6c site. However, such behaviour is absent when H_2O is adsorbed on Ti-5c or Ti-4c site of $aTiO_2$ surface. This reconstruction of the surface due to the presence of water in the vicinity of Ti-6c site is probably the reason H_2O is more stable on Ti-6c site compared to Ti-5c and Ti-4c site of $aTiO_2$ surface.

By comparing water adsorption on pristine $aTiO_2$ with water adsorption on rutile (1 1 0) surface (Table 1), it is clear that water is slightly more stable on sixfold coordinated Ti atom of $aTiO_2$ surface then on fivefold coordinated Ti atom of rutile (1 1 0) surface (Table 1), with a difference of about 0.13 eV in their adsorption energies. Further, the bond distance analysis shows that water adsorbs on the Ti-6c site with a 3.52 Å distance between the surface Ti atom and the O atom of water, which is higher than the existing experimental measurements (2.21±0.02 Å) [40] as well as our theoretical calculations for water adsorption on rutile (1 1 0) surface. The strongest adsorption energy and higher distance of water from the $aTiO_2$ surface indicate that $aTiO_2$ can be used to achieve highly stable anchoring of water contrary to crystalline surface on which water is comparatively less stable but chemically bonded. Furthermore, after dissociation of water on $aTiO_2$ surface, the most stable configration is the one in which the OH group binds to the fourfold coordinated Ti atom while the remaining H atom binds with the O atom coordinated to fourfold Ti. This indicates that even though the molecular adsorption of water is more probable at sixfold coordinated Ti atom, the dissociative adsorption of water might take place at under-coordinated surface Ti atom as on $cTiO_2$ catalyst.

In order to understand water dissociation on Fe(II)-$aTiO_2$ surface author then optimized three different configurations representing Fe(II)-$aTiO_2$ surface: Fe(II) doped at Ti-4c site (Fe(II)-4c-$aTiO_2$), Fe(II) doped at Ti-5c site (Fe(II)-5c-$aTiO_2$) and Fe(II) doped at Ti-6c site (Fe(II)-6c-$aTiO_2$) (Figure 3). In all these surface +2 oxidation state of Fe is achieved by substituting one Ti and one O atom with one Fe atom. Out of these three surfaces Fe(II)-6c-$aTiO_2$ was the most stable surface with total energy difference of −1.37 and −1.13 eV from Fe(II)-5c-$aTiO_2$ and Fe(II)-4c-$aTiO_2$ surfaces, respectively. Further, the spin density plot for the doped system (Figure 5(b)) shows that the spin densities are strongly localized on the Fe atom and O sites in the nearest-neighbour position relative to the Fe dopant.

Next, water adsorption on the most stable, Fe(II)-6c-$aTiO_2$, surface was analysed. The adsorption of H_2O molecule was analysed by placing it on the top of Fe atom, resulting in the binding energy of −0.79 eV. Comparing with pristine $aTiO_2$ and rutile (1 1 0) surfaces, H_2O is energetically least stable on Fe(II)-$aTiO_2$ surface. However, the distance (2.26 Å) between the Fe atom of the surface and the O atom of the water molecule is similar to the distance (2.21 Å) of adsorbed water on rutile (1 1 0) surface. Further, the author performed calculations for OH and H adsorption on Fe(II)-6c-$aTiO_2$ surface by placing OH on the top of Fe atom and H on top of four different O atom sites indicated by g, c, d and e in Figure 3. As for H_2O adsorption, OH and H adsorption is also less stable when compared to OH and H adsorption on pristine $aTiO_2$ surface. The binding energy and vertical distance analysis indicate the Fe(II)-$aTiO_2$ surface might behave similarly to $cTiO_2$ surfaces for water adsorption and dissociation.

3.3. Reaction pathway for water dissociation

In order to gain an atomic scale understanding of the fundamental reaction pathway and get a sense of the relative activation energy barriers faced during water dissociation, CI-NEB calculations with 7 images were performed for all the surfaces. The preliminary results for the MEP and the TS energies for water dissociation on $aTiO_2$, Fe(II)-$aTiO_2$ and rutile (1 1 0) surfaces are

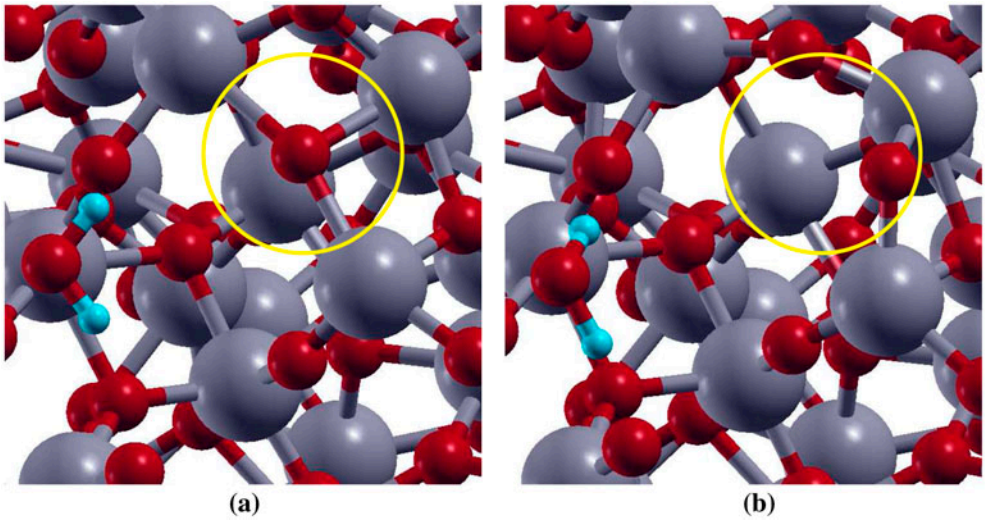

Figure 4. Top view representation of H_2O adsorption on $aTiO_2$ surface (a) before, and (b) after optimization. Ti and O atoms are represented by grey, and red balls, respectively.

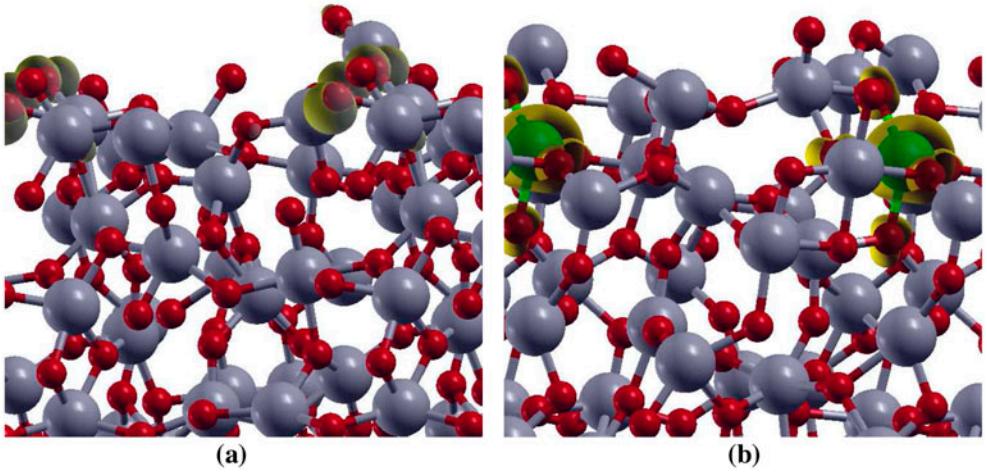

Figure 5. The spin density ($\rho\uparrow - \rho\downarrow$) for (a) undoped $aTiO_2$, and (b) Fe(II)-$aTiO_2$ surface models. The isovalue used for spin density plots is 0.005 eÅ^{-3}. Ti, Fe, and O atoms are represented by grey, green and red balls, respectively. The spin density isosurface is represented in yellow color.

represented in Figures 6–8, respectively, along with the initial state (IS), TS, and final state (FS) geometries. The chosen TS configration corresponds to the highest energy point along the MEP. The activation energy barrier, E_a, is calculated as $E_a = E_{TS} - E_{IS}$, and the reaction energy, ΔE is calculated as $\Delta E = E_{FS} - E_{IS}$, where E_{TS} is the energy of the TS, E_{IS} is the energy of IS and E_{FS} is the energy of the FS. The negative ΔE indicates an exothermic reaction and a positive ΔE represents an endothermic one. Based on the most stable water adsorption sites (Table 1), Ti-4c, Ti-6c and Ti-5c sites were chosen for water dissociation on $aTiO_2$, Fe-$aTiO_2$ and rutile (1 1 0) surfaces, respectively. The IS corresponds to surface with chemically adsorbed H_2O molecule, and the FS corresponds to the surfaces having dissociated water molecule with OH and H species adsorbed on the surface.

The reaction path was found to have similar TSs for both Fe(II)-$aTiO_2$ (Figure 7), and rutile (1 1 0) (Figure 8) surfaces [39], where the H_2O molecule gets distorted resulting in elongated OH–H bond. However, for pristine $aTiO_2$ surface TS consists of dissociated H_2O molecule with OH and H group bonded to the surface Ti and O atoms, respectively. Furthermore, our calculations of reaction energy, ΔE, indicate that water dissociation is exothermic on $aTiO_2$ ($\Delta E = -3.09$ eV) and Fe(II)-$aTiO_2$ ($\Delta E = -1.27$ eV) surfaces just like that on rutile (1 1 0) ($\Delta E = -0.84$) surface and other $cTiO_2$ surfaces [41]. It should also be noted that, water splitting on Fe(II)-$aTiO_2$ surface is less exothermic than on $aTiO_2$ surface and more exothermic than on $cTiO_2$ surfaces. The negative reaction energies for $aTiO_2$-based catalysts point towards favorable kinetics.

Further, the H_2O dissociation is spontaneous on the rutile (1 1 0) surface but faces certain barrier for dissociation on amorphous surfaces. Activation energy barrier (E_a) analyses shows that water dissociation on pristine $aTiO_2$ and Fe(II)-$aTiO_2$ surfaces has E_a of 0.92

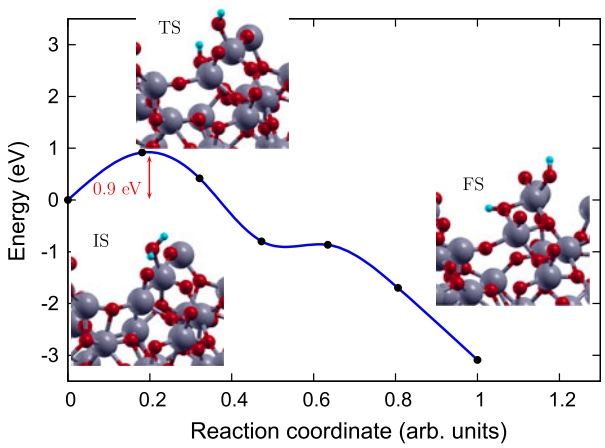

Figure 6. Reaction pathway and reaction barrier for dissociation of single water molecule on pristine $aTiO_2$ surface from CI-NEB simulation. Ti, O, and H atoms are highlighted in grey, red, and light blue, respectively.

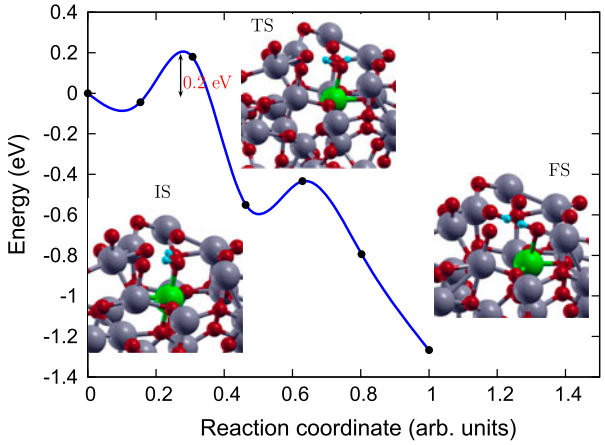

Figure 7. Reaction pathway and reaction barrier of single water molecule dissociation on Fe(II)-$aTiO_2$ surface from CI-NEB simulation. Ti, O, Fe and H atoms are highlighted in grey, red, green and light blue, respectively.

and 0.18 eV, making Fe(II)-$aTiO_2$ surface energetically more favourable for water splitting compared to pristine $aTiO_2$ surface. The smaller activation barrier for water dissociation on the Fe(II)-$aTiO_2$ surface is due to its unique band structure Figure 2. The tail states present in Fe(II)-$aTiO_2$ band structure (Figure 2(b)) might lead to better hybridization of energy states of the H_2O molecule with the energy states of Fe(II)-$aTiO_2$ surface than the energy states of the pristine $aTiO_2$ surface. In other words, the existence of these resonating energy states in Fe(II)-$aTiO_2$ catalyst might make it easier for the H atom of the H_2O molecule to bind with the neighbouring O atom of the surface upon H_2O molecule interaction with the Fe-$aTiO_2$ surface.

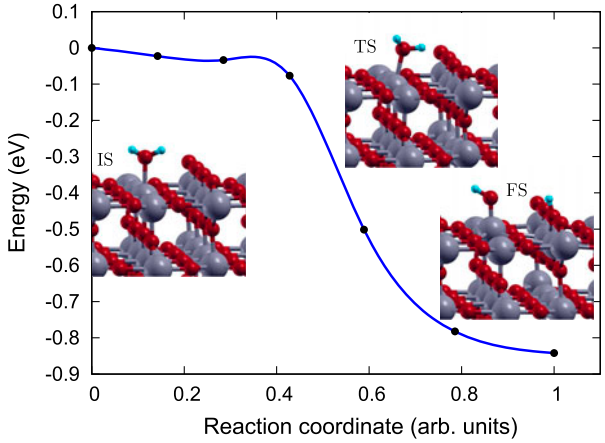

Figure 8. Reaction pathway and reaction barrier of single water molecule dissociation on rutile (1 1 0) surface from CI-NEB simulation. Ti, O, and H atoms are highlighted in grey, red, and light blue, respectively.

4. Conclusions

In this study, DFT+U analysis was conducted for providing the mechanistic insights into the water splitting reaction on the $aTiO_2$-based catalysts. Our analysis showed that in contrast to crystalline surfaces H_2O molecule tends to be more stable on sixfold coordinated Ti site then on under-coordinated sites of $aTiO_2$ surface. Further, the interaction between H_2O and sixfold Ti site of $aTiO_2$ surface is stronger ($\delta H_{ads} = -1.07$ eV) than the interaction between H_2O and fivefold Ti site of rutile (1 1 0) surface ($\delta H_{ads} = -0.94$ eV). The higher H_2O stability on the pristine $aTiO_2$ surface could be attributed to the difference in the surface states of the adsorption sites where the spatial arrangement of the O atoms with reference to the Ti atom plays a major role. Furthermore, the density of states analyses and the CI-NEB analysis conducted in this study points towards better photocatalytic activity of doped $aTiO_2$ as compared to pristine $aTiO_2$ for water splitting. Overall, the present study reinforces the usefulness of doping in amorphous TiO_2 catalysts providing an alternative path to prepare an efficient and cost-effective visible light photocatalysts.

Acknowledgements

This project was supported by JSPS and NSF under the JSPS-NSF Partnerships for International Research and Education (PIRE).

Disclosure statement

No potential conflict of interest was reported by the authors.

Funding

This work was supported by the International Institute for Carbon Neutral Energy Research (WPI-I^2CNER), sponsored by the World Premier International Research Center Initiative (WPI), MEXT, Japan. The computations were performed by using Research Center for Computational Science, Okazaki, Japan and the HPC supercomputers at International Institute for Carbon Neutral Energy Research (I^2CNER), Kyushu University, Japan.

References

[1] Wu NQ, Wang J, Tafen DN, et al. Shape-enhanced photocatalytic activity of single-crystalline anatase TiO_2 (101) nanobelts. J Am Chem Soc. 2010;132:6679.

[2] Yu J, Yu JC, Leung MKP, et al. Effects of acidic and basic hydrolysis catalysts on the photocatalytic activity and microstructures of bimodal mesoporous titania. J Catal. 2007;217:69.

[3] Sato R, Shibuta Y, Shimojo F, et al. Effects of CO_2 adsorption on proton migration on a hydrated ZrO_2 surface: an ab initio molecular dynamics study. Phys Chem Chem Phys. 2017;19:20198–20205.

[4] Morgan BJ, Watson GW. Polaronic trapping of electrons and holes by native defects in anatase TiO_2. Phys Rev B. 2009 Dec;80:233102. DOI:10.1103/PhysRevB.80.233102

[5] Di Valentin C, Pacchioni G, Selloni A. Origin of the different photoactivity of *n*-doped anatase and rutile TiO_2. Phys Rev B. 2004;70(8):085116.

[6] Landmann M, Rauls E, Schmidt WG. The electronic structure and optical response of rutile, anatase and brookite TiO_2. J Phys Condensed Matter. 2012;24(19):195503. Available from: http://stacks.iop.org/0953-8984/24/i=19/a=195503

[7] Kandemir EB, Gonul B, Barkema G, et al. Modeling of the atomic structure and electronic properties of amorphous GaN1-xAsx. Comput Mater Sci. 2014;82:100. Available from: http://www.sciencedirect.com/science/article/pii/S0927025613005740

[8] Zhang H, Chen B, Banfield JF, et al. Atomic structure of nanometer-sized amorphous TiO_2. Phys Rev B. 2008 Dec;78:214106. DOI:10.1103/PhysRevB.78.214106

[9] Standridge SD, Schatz GC, Hupp JT. Toward plasmonic solar cells: protection of silver nanoparticles via atomic layer deposition of TiO_2. Langmuir. 2009;25(5):2596. DOI:10.1021/la900113e

[10] Prasai B, Cai B, Drabold DA. Ab-initio calculation of structural and electrical properties of amorphous TiO_2. MS&T-11 Conference of Proceedings. 2011.

[11] Stromme M, Ahuja R, Niklasson GA. New probe of the electronic structure of amorphous materials. Phys Rev Lett. 2004;93:206403.

[12] Kaur K, Singh CV. Amorphous TiO_2 as a photocatalyst for hydrogen production: a DFT study of structural and electronic properties. Energy Procedia. 2012;29:291.

[13] Pham HH, Wang LW. Oxygen vacancy and hole conduction in amorphous TiO_2. Phys Chem Chem Phys. 2015;17:541.

[14] Griscom DL. Self-trapped holes in amorphous silicon dioxide. Phys Rev B. 1989 Aug;40:4224. DOI:10.1103/PhysRevB.40.4224

[15] Itoh N, Shimizu-Iwayama T, Fujita T. Excitons in crystalline and amorphous SiO_2: formation, relaxation and conversion to frenkel pairs. J Non-Cryst Solids. 1994;179:194. Available from: http://www.sciencedirect.com/science/article/pii/0022309394906971

[16] Hayes W, Jenkin TJL. Charge-trapping properties of germanium in crystalline quartz. J Phys C: Solid State Phys. 1986;19(31):6211. Available from: http://stacks.iop.org/0022-3719/19/i=31/a=015

[17] Buddee S, Wongnawa S, Sirimahachai U, et al. Recyclable UV and visible light photocatalytically active amorphous TiO_2 doped with M (III) ions (M = CR and Fe). Mater Chem Phys. 2011;126:167.

[18] Prasai B, Cai B, Underwood MK, et al. Properties of amorphous and crystalline titanium dioxide from first principles. J Mater Sci. 2012;47:7515.

[19] Zhang Z, Maggard PA. Investigation of photocatalytically-active hydrated forms of amorphous titania $TiO_2.nH_2O$. J Photochem Photobiol A: Chem. 2007;186:8.

[20] Li J, Liu S, He Y, et al. Adsorption and degradation of the cationic dyes over Co doped amorphous mesoporous titania-silica catalyst under UV and visible light irradiation. Micropor Mesopor Mater. 2008;115:416.

[21] Kanna M, Wongnawa S. Mixed amorphous and nanocrystalline TiO_2 powders prepared by sol-gel method: characterization and photocatalytic study. Mater Chem Phys. 2008;110:166.

[22] Ghuman KK, Singh CV. Effect of doping on electronic structure and photocatalytic behavior of amorphous TiO_2. J Phys: Condens Matter. 2013;25:475501.

[23] Chen X, Liu L, Yu PY, et al. Increasing solar absorption for photocatalysis with black hydrogenated titanium dioxide nanocrystals. Science. 2011;331:746.

[24] Ghuman KK, Singh CV. Self-trapped charge carriers in defected amorphous TiO_2. J Phys Chem C. 2016;120(49):27910. DOI:10.1021/acs.jpcc.6b07326

[25] Kaur K, Prakash S, Goyal N. Strained structure of differently prepared amorphous TiO_2 nanoparticle: molecular dynamics study. J Mater Res. 2011;26:2604.

[26] Hung WC, Fu SH, Tseng JJ, et al. Study on photocatalytic degradation of gaseous dichloromethane using pure and iron ion-doped TiO_2 prepared by the sol-gel method. Chemosphere. 2007;66:2142.

[27] George S, Pokhrel S, Ji Z, et al. Role of fe doping in tuning the band gap of TiO_2 for the photo-oxidation-induced cytotoxicity paradigm. J Am Chem Soc. 2011;133(29):11270. DOI:10.1021/ja202836s

[28] Perdew J, Burke K, Ernzerhof M. Generalized gradient approximation made simple. Phys Rev Lett. 1996;77:3865.

[29] Vanderbilt D. Soft self-consistent pseudopotentials in a generalized eigenvalue formalism. Phys Rev B. 1990;41(11):7892.

[30] Giannozzi P, Baroni S, Bonini N, et al. Quantum espresso: a modular and open-source software project for quantum simulations of materials. J Phys: Condens Matter. 2009;21:395502.

[31] Deskins NA, Dupuis M. Electron transport via polaron hopping in bulk TiO_2: a density functional theory characterization. Phys Rev B. 2007;75:195212.

[32] Ghuman KK, Singh CV. A DFT + U study of (Rh, Nb)-codoped rutile $TiO_{(2)}$. J Phys: Condens Matter. 2013;25:085501.

[33] Morgan BJ, Watson GW. A DFT+U description of oxygen vacancies at the TiO_2 rutile (1 1 0) surface. Surf Sci. 2007;601:5034.

[34] Chen QL, Li B, Zheng G, et al. First-principles calculations on electronic structures of fe-vacancy-codoped $TiO_{(2)}$ anatase (101) surface. Physica B. 2011;406:3841.

[35] Norton DP. Synthesis and properties of epitaxial electronic oxide thin-film materials. Mater Sci Eng R Rep. 2004;43(5–6):139–247.

[36] Mills G, Jonsson H, Schenter GK. Reversible work transition state theory: application to dissociative adsorption of hydrogen. Surf Sci. 1995;324:305.

[37] Jonsson H, Mills G, Jacobsen KW. In: Berne BJ, Ciccotti G, Coker DF, editors. Classical and quantum dynamics

in condensed phase simulations. Singapore: World Scientific; 1998.
[38] Henkelman G, Jonsson HG. Improved tangent estimate in the nudged elastic band method for finding minimum energy paths and saddle points. J Chem Phys. 2000;113:9978.
[39] Miao M, Liu Y, Wang Q, et al. Activation of water on the TiO_2 (110) surface: the case of ti adatoms. J Chem Phys. 2012;136:064703.
[40] Allegretti F, O'Brien S, Polcik M, et al. Adsorption bond length for H_2O on TiO_2(1 1 0): a key parameter for theoretical understanding. Phys Rev Lett. 2005 Nov;95:226104. DOI:10.1103/PhysRevLett.95.226104
[41] Ji Y, Wang B, Luo Y. GGA+U study on the mechanism of photodecomposition of water adsorbed on rutile TiO_2 (110) surface: free vs. trapped hole. J Phys Chem C. 2014;118(2):1027. DOI:10.1021/jp409605y